Bulk superconductivity in Pb-substituted BiS_2-based compounds studied by hard x-ray spectroscopy

A. Yamasaki,[1,2,*] T. Oguni,[3] T. Hayashida,[2,3] K. Miyazaki,[2,3] N. Tanaka,[2,3] K. Nakagawa,[2,3] K. Tamura,[4] K. Mimura,[4,5] N. Kawamura,[6] H. Fujiwara,[2,7,8] G. Nozue,[2,7] A. Ose,[2,7] Y. Kanai-Nakata,[2,9] A. Higashiya,[2,10] S. Hamamoto,[2] K. Tamasaku,[2] M. Yabashi,[2] T. Ishikawa,[2] S. Imada,[2,9] A. Sekiyama,[2,7,8] H. Sakata,[11] and S. Demura[12]

[1]*Faculty of Science and Engineering, Konan University, Kobe 658-8501, Japan*
[2]*RIKEN SPring-8 Center, Sayo, Hyogo 679-5148, Japan*
[3]*Graduate School of Natural Science, Konan University, Kobe 658-8501, Japan*
[4]*Graduate School of Engineering, Osaka Prefecture University, Sakai, Osaka 599-8531, Japan*
[5]*Graduate School of Engineering, Osaka Metropolitan University, Sakai, Osaka 599-8531, Japan*
[6]*Japan Synchrotron Radiation Research Institute, Sayo, Hyogo 679-5198, Japan*
[7]*Graduate School of Engineering Science, Osaka University, Toyonaka, Osaka 560-8531, Japan*
[8]*Spintronics Research Network Division, Institute for Open and Transdisciplinary Research Initiatives, Osaka University, Suita, Osaka 565-0871, Japan*
[9]*College of Science and Engineering, Ritsumeikan University, Kusatsu, Shiga 525-8577, Japan*
[10]*Faculty of Science and Engineering, Setsunan University, Neyagawa, Osaka 572-8508, Japan*
[11]*Department of Physics, Tokyo University of Science, Tokyo 162-8601, Japan*
[12]*College of Science and Technology, Nihon University, Tokyo 101-8308, Japan*

(Received 26 May 2023; revised 24 November 2023; accepted 2 January 2024; published 17 January 2024)

In this study, we investigate the bulk electronic structure of Pb-substituted $LaO_{0.5}F_{0.5}BiS_2$ single crystals, using two types of hard x-ray spectroscopy. High-energy-resolution fluorescence-detected x-ray absorption spectroscopy revealed a spectral change at low temperatures. Using density functional theory (DFT) simulations, we find that the temperature-induced change originates from a structural phase transition, similar to the pressure-induced transition in $LaO_{0.5}F_{0.5}BiS_2$. This finding suggests that the mechanism of bulk superconductivity induced by Pb substitution is the same as that under high pressure. Furthermore, a low-valence state with a mixture of divalent and trivalent Bi ions is discovered using hard x-ray photoemission spectroscopy with the aid of DFT calculations.

DOI: 10.1103/PhysRevB.109.045131

I. INTRODUCTION

More than 20 years have passed since the beginning of the 21st century, during which several superconductors have been discovered [1]. In this period, the concept that the phase of the wave function governs some physical properties led to a whole new category of materials called topological materials [2]. These two fields converged in the search for topological superconductors. Then, the proposed candidate materials such as $Cu_xBi_2Se_3$ initiated a new trend in superconductor research [3,4]. Alongside this trend, another Bi-based superconductor, $LaO_{1-x}F_xBiS_2$, was discovered in 2012 [5]. It has a stacking structure consisting of two-dimensional superconducting planes and blocking layers, similar to unconventional superconductors such as cuprates discovered in the 20th century and later iron-based superconductors [6]. Unlike them, however, the material has a pyramidal coordination structure with C_{4v} symmetry group at the Bi site, breaking the local inversion symmetry. In addition, the $6p$ electrons in the outermost shell of the Bi atom, which are responsible for the superconductivity in this system [7], exhibit a spin-orbit interaction that is an order of magnitude stronger than that of the $3d$ electrons in Cu and Fe. The strong spin-orbit interaction induces a large Rashba splitting owing to the spatial inversion symmetry breaking [8]. This spin-dependent splitting is, however, compensated for by the upper and lower BiS layers, resulting in spin-degenerate bulk bands that mask the unique nature of the system [9].

Nevertheless, an unusual property, i.e., anisotropic upper critical field beyond the Pauli limit, has recently been reported in the BiS_2-based superconductors [10,11]. Together with other experimental results suggesting unconventional superconductivity and a new pairing mechanism [12,13], this has generated considerable interest in the field. While the family of BiS_2-based superconductors has expanded as a result of extensive research, a systematic understanding linking the following points has not yet been fully established [14,15]: (i) changes in transition temperatures and superconducting volume fractions due to pressure application and element substitution, (ii) microscopic understanding of the flatness of the BiS plane and the symmetry of the Bi sites, and (iii) whether the superconducting mechanism is conventional or unconventional.

In $LaO_{0.5}F_{0.5}BiS_2$, electron doping of the BiS planes by F substitutions on the O sites of the semiconducting $LaOBiS_2$ induces superconductivity with a critical temperature $T_c \simeq 3$ K [14]. The resulting superconductivity is known

*Corresponding author: yamasaki@konan-u.ac.jp

to be filamentary with a very low superconducting volume fraction. Similar to many other BiS_2-based superconductors, this material crystallizes in a tetragonal crystal belonging to the space group $P4/nmm$. Bulk superconductivity can be observed by substitution on chalcogen and rare-earth sites, but there is no significant increase in T_c [16–19]. On the other hand, under high pressure, it exhibits bulk superconductivity with the highest T_c of 11 K in the family, and the crystal structure changes to an orthorhombic crystal belonging to the space group $P2_1/m$ [20]. Previous studies have suggested that this temperature-induced structural phase transition may even change the mechanism of superconductivity [21]. The presence of two adjacent superconducting phases, conventional and unconventional, makes it difficult to understand the superconductivity of this system.

Recently, it has been reported that bulk superconductivity appears at relatively low Pb concentrations (8%–9%) after the disappearance of filamentary superconductivity when the key element for superconductivity, Bi, is partially replaced by Pb [22]. It is still unclear whether the superconductivity induced by the elemental substitution at the Bi site differs from that in other elemental substitution systems. In the narrow concentration range of Pb, where bulk superconductivity appears, a cusp-shaped electrical resistivity anomaly is observed around 100 K, which is not found in other BiS_2 systems. This anomaly is of interest in the context of superconductivity.

In this study, we investigate the bulk electronic structure of $LaO_{0.5}F_{0.5}Bi_{1-x}Pb_xS_2$ single crystals with the above Pb concentration using two types of hard x-ray spectroscopy: x-ray absorption spectroscopy and photoemission spectroscopy. Our goal is to gain insight into the bulk superconductivity and the anomaly around 100 K induced by Pb substitution. To reveal subtle temperature changes in the electronic structures, we use a high-energy-resolution fluorescence detection mode for x-ray absorption near edge structure (HERFD-XANES), which can suppress the lifetime broadening effect in the spectrum. Density functional theory (DFT) simulations show that the spectral change is explained by a temperature-induced structural phase transition, suggesting that the bulk superconductivity is driven by a mechanism similar to that in the high-pressure phase of $LaO_{0.5}F_{0.5}BiS_2$. Hard x-ray photoemission spectroscopy (HAXPES) results for the Bi valence are in good agreement with the DFT results, indicating the observation of a low-valence state with a mixture of divalent and trivalent Bi ions.

II. EXPERIMENTAL

Single crystals of $LaO_{0.5}F_{0.5}Bi_{1-x}Pb_xS_2$ ($x = 0$, 0.05, 0.09) and $LaOBiS_2$ were grown by a flux method using CsCl and KCl as flux materials, where x is the nominal content. Filamentary and bulk superconductivity appeared at 3 K for $x = 0$ and 4 K for $x = 0.09$, respectively, while no superconductivity above 2 K was observed for $x = 0.05$. Details of the sample preparation and their properties have been reported elsewhere [22]. In these compounds, the typical crystal size was about 1.5 mm × 1.5 mm × 0.1 mm. The crystal structures were determined by powder x-ray diffraction (XRD) at the beamline BL02B2 of SPring-8. In the case of $x = 0$ (0.08), the lattice constants a and c, analyzed by the Rietveld method based on the space group $P4/nmm$, were 4.06263 Å and 13.51420 Å (4.06451 Å and 13.47650 Å), respectively [23]. Because of the narrow range of Pb concentration at which the compound exhibits bulk superconductivity, crystals grown even in the same batch may have different characteristics. In this study, crystals with $x = 0.09$ were selected for spectroscopic experiments on the basis of the (004) peak position of the laboratory-XRD profile, which is closely related to the value of the diamagnetic susceptibility at low temperatures [22].

The HERFD-XANES experiments were performed at the beamline BL39XU of SPring-8 [24]. The incident x-ray beam was delivered by the planar undulator and monochromized by the Si(220) double-crystal monochromator. The fluorescence intensity of Bi and Pb $L\alpha_1$ main lines, selected by the Si(911) crystal-analyzer spectrometer, was monitored using the two-dimensional pixel detector PILATUS while sweeping the incident photon energy around Bi and Pb L_3 absorption edges. The $L\alpha_1$ fluorescence detection overcomes the common L_3-edge lifetime broadening (∼5.9 eV) known as the natural linewidth and provides a spectrum with higher energy resolution [24,25]. The energy resolution estimated from an elastic scattering peak near the Bi $L\alpha_1$ line was 1.1 eV as the full width at half maximum (FWHM), while the lifetime broadening is about 2.9 eV. In addition, the conventional L_3-edge XANES spectrum was simultaneously recorded by the partial fluorescence yield (PFY) mode using a silicon drift detector.

The HAXPES experiments were performed at the beamline BL19LXU of SPring-8 [26]. The linearly polarized x-ray was delivered by the 27-m-long undulator, and monochromized by the Si(111) double-crystal and Si(620) channel-cut monochromators. The polarization direction was set to be parallel to the photoelectron scattering plane (referred to as p polarization) [27]. The incident photon energy and total energy resolution were set to 7.9 keV and 300 meV (FWHM), respectively. Along the entrance slit, photoelectrons emitted within approximately ±10 deg of normal to the sample surface were detected by the MB Scientific A-1 HE spectrometer using the A1L2 lens in HE12 mode [28]. Clean (001) surfaces were obtained by cleaving the samples *in situ* in ultrahigh vacuum ($\lesssim 1 \times 10^{-7}$ Pa). The Fermi energy (E_F) was determined from the photoemission spectra of evaporated gold films.

To reproduce the spectra, we performed scalar-relativistic DFT calculations using the WIEN2K code [29]. The local spin density approximation plus spin-orbit coupling was used in the calculations. For the DFT calculations of $LaO_{0.5}F_{0.5}BiS_2$ in the high-pressure (HP) phase and $LaOBiS_2$, the lattice constants and atomic coordinates have been taken from Refs. [20] and [30].

III. RESULTS AND DISCUSSION

A. HERFD XANES

Figure 1(a) shows Bi L_3-edge XANES spectra of $LaO_{0.5}F_{0.5}Bi_{1-x}Pb_xS_2$ for $x = 0$, 0.05, and 0.09 recorded at 200 K using two different techniques, the conventional PFY and the HERFD modes. In contrast to the featureless and rather broadened PFY spectra, some fine structures are

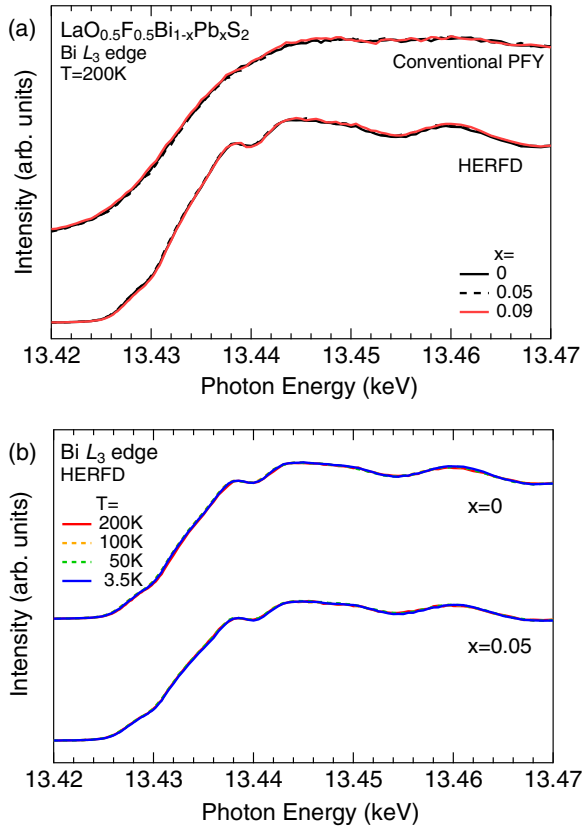

FIG. 1. (a) Bi $L\alpha_1$ HERFD-XANES spectra for $x = 0$, 0.05, and 0.09 at 200 K. Simultaneously measured conventional PFY spectra are also displayed. (b) Temperature dependence of Bi $L\alpha_1$ HERFD-XANES spectra for $x = 0$ and 0.05.

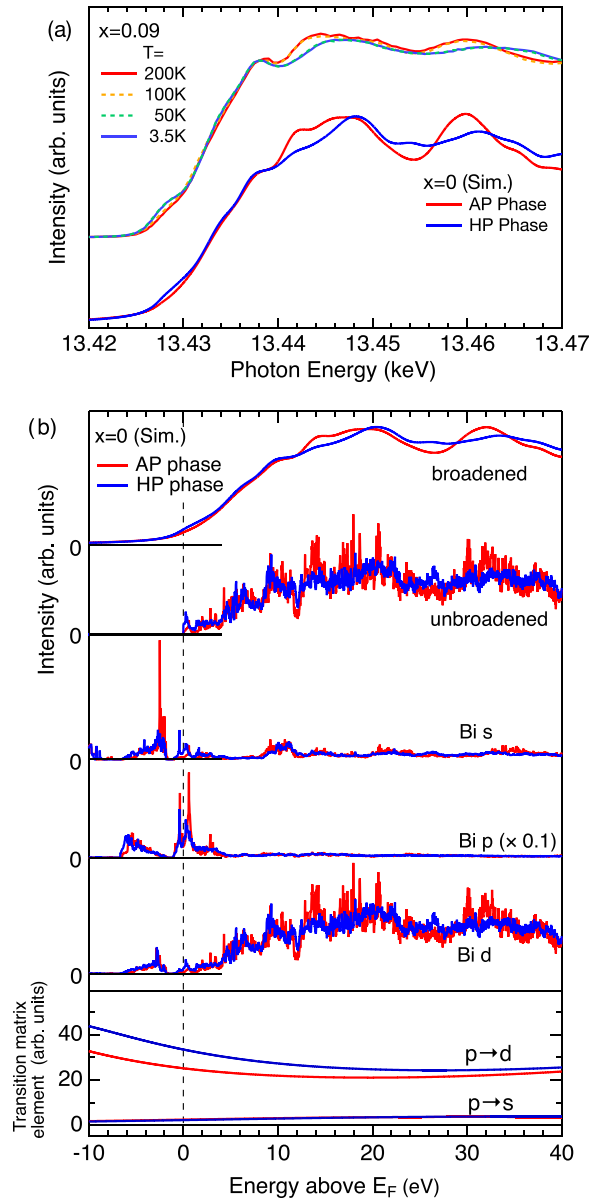

FIG. 2. Experimental and simulated Bi L_3-edge XANES spectra of $LaO_{0.5}F_{0.5}Bi_{1-x}Pb_xS_2$. (a) Temperature dependence of Bi $L\alpha_1$ HERFD-XANES spectrum for $x = 0.09$. Simulated spectra for $x = 0$ in the AP and HP phases are shown for comparison. The simulated spectra are broadened by Gaussian and Lorentzian functions representing the experimental energy-resolution and lifetime effects. (b) Details of the simulated spectra in (a). These are composed of unoccupied Bi s- and d-orbital pDOSs after multiplying the transition probabilities. The Bi p-orbital pDOS is also shown for reference.

resolved in the HERFD spectra. Meanwhile, the spectra for $x = 0$, 0.05, and 0.09 are barely distinguishable from one another in both modes. The temperature dependence of the HERFD-XANES spectra for $x = 0$ and 0.05 is shown in Fig. 1(b). The spectra do not show any temperature dependence. In contrast, Fig. 2(a) shows that the spectral shape at $x = 0.09$ changes significantly between 100 and 50 K. The temperature range in which the spectral change was observed includes the temperature at which the cusp-shaped anomaly in the $\rho - T$ curve was observed [22]. In addition, a synchrotron-XRD experiment has recently demonstrated the peak splitting in the profile for $x = 0.09$ below about 100 K [23], suggesting the structural transition of the crystal with the symmetry lowering.

To reproduce the temperature dependence of the HERFD-XANES spectrum for $x = 0.09$, we performed DFT calculations and simulated the spectra using the XSPEC program [31,32]. Since details of the crystal structure of the low-T phase for $x = 0.09$ are not yet known, we assumed here that the phase has the same crystal structure, i.e., the same lattice constants and atomic coordinates, as the HP phase for $x = 0$ with the space group $P2_1/m$, based on the experimental evidence: high superconducting volume fraction and high T_c in both phases [20]. In addition, since the spectral shapes of $x = 0$ and 0.09 at high temperatures are very similar as seen in Fig. 1(a), the crystal structure of $x = 0$ in the ambient-pressure (AP) phase is used for comparison instead of that of $x = 0.09$. The simulated XANES spectra are shown in Figs. 2(a) and 2(b). The total difference induced by the temperature change is well reproduced by the simulation, indicating that the temperature-induced change originates from a structural phase transition, similar to the pressure-induced transition in $LaO_{0.5}F_{0.5}BiS_2$. This suggests that the mechanism of bulk superconductivity induced by Pb substitution is the same as that under high pressure. In the Bi L_3-edge

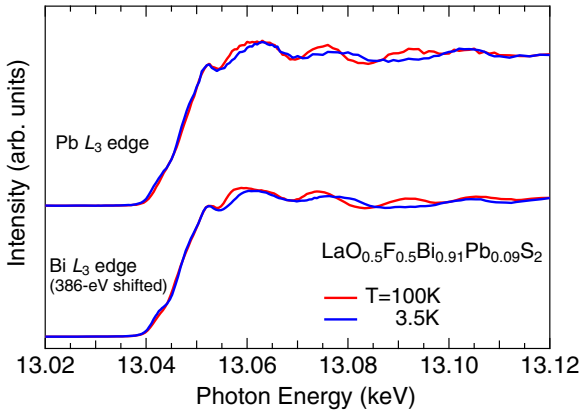

FIG. 3. Temperature dependence of Pb $L\alpha_1$ HERFD-XANES spectrum for $x = 0.09$. Bi $L\alpha_1$ HERFD-XANES spectra (shifted) are also shown for comparison.

absorption process, the electrical dipole transition from $2p$ to $6d$ states becomes dominant, as can be seen at the bottom of Fig. 2(b). Therefore, the XANES spectra mainly reflect unoccupied Bi $6d$ states depending on their crystal structures, although one can also find a structural-induced change at the absorption threshold in Bi $6s$ states.

We also investigated the Pb-derived electronic states. Figure 3 shows the temperature variation of the Pb $L\alpha_1$ HERFD-XANES spectrum for $x = 0.09$. The spectral shape and the temperature-induced change observed here are very similar to those seen in the spectrum for the Bi L_3 edge, indicating that substituted Pb atoms properly occupy the Bi lattice site.

B. Core-level HAXPES

The Bi- and Pb-derived electronic states were further investigated by HAXPES, which is a complementary method for probing bulk electronic structures. Bi $4f$ core-level HAXPES spectra of $LaOBiS_2$ and $LaO_{0.5}F_{0.5}Bi_{1-x}Pb_xS_2$ for $x = 0$ and 0.09 are shown in Fig. 4(a). $LaOBiS_2$ has a single-peak-like structure in both the Bi $4f_{7/2}$ and $4f_{5/2}$ states, as observed in the soft x-ray photoemission spectroscopy (SXPES) study [34]. In contrast, a double-peak structure with stronger intensity of the lower-binding energy (E_B) peak was observed for $x = 0$. This characteristic feature in the HAXPES spectrum is quite different from that seen in the SXPES spectrum, which has the single-peak structure with a weak shoulder on the lower-E_B side. Such a difference is often observed in some correlated materials where the electron correlation effects are enhanced at the surface. Owing to the long inelastic mean free path of emitted photoelectrons [35], HAXPES provides highly bulk sensitive information, resulting in a significant intensity of the nonlocally screened *final* state in the spectrum for these materials [36]. However, it should be noted that BiS_2-based compounds are considered to be an itinerant electron system, as the highly dispersive Bi $6p$ bands cross the E_F in the metallic state and play a key role in the low-energy phenomena such as superconductivity [7]. In this case, it is reasonable to assume that the double-peak structure observed in the Bi $4f$ core level consists of two states with different valences

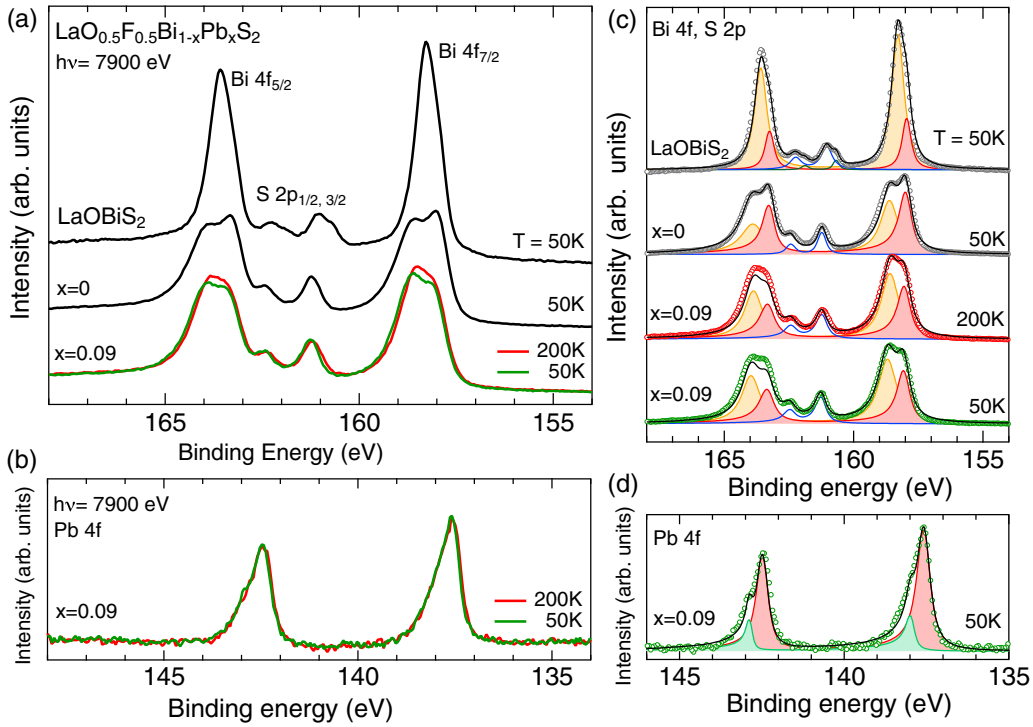

FIG. 4. Bi and Pb $4f$ core-level HAXPES spectra of $LaO_{0.5}F_{0.5}Bi_{1-x}Pb_xS_2$. The spectra are normalized by the area under the curves after subtraction of the Shirley-type background [33]. (a) Bi $4f$ core-level HAXPES spectra, including the S $2p$ core levels, for $x = 0$ and 0.09. The spectrum of $LaOBiS_2$ is also shown. (b) The temperature dependence of the Pb $4f$ core-level HAXPES spectrum for $x = 0.09$. (c) and (d) The results of the line-shape analysis for the HAXPES spectra.

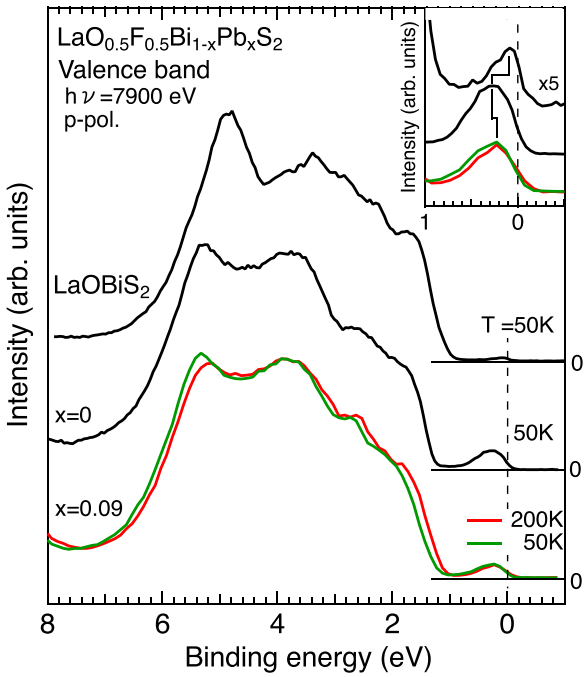

FIG. 5. VB-HAXPES spectra of $LaO_{0.5}F_{0.5}Bi_{1-x}Pb_xS_2$. The spectrum of $LaOBiS_2$ is also shown. The inset shows the enlarged spectra near E_F. The spectra are normalized by the area under the curves after subtraction of the Shirley-type background.

in the *initial* state, as in other Bi compounds [37,38]. Thus, the spectral change resulting from the F (Pb) substitution to the O (Bi) site can be understood in terms of the electron (hole) doping effect. As for $x = 0.09$, the lower-E_B peak is suppressed by the Pb substitution in the double-peak structure, which becomes slightly broader and shifts (∼50 meV) with decreasing temperature.

Line-shape analysis shows that the spectral shape of each of the Bi $4f_{7/2}$ or $4f_{5/2}$ states in all three compounds can be accurately reproduced by two Voigtian peaks, as shown in Fig. 4(c). Although Bi ions tend to be neutral, trivalent, and pentavalent, the lower-E_B (higher-E_B) component is assumed to be derived from the divalent (trivalent) state by considering the following facts: (i) the nominal valence of Bi ions for semiconducting $LaOBiS_2$ is +3. (ii) The valence-band (VB) HAXPES spectrum of $LaOBiS_2$ shown in the inset of Fig. 5 indicates that a small amount of electrons are doped to Bi $6p$ bands, possibly owing to some oxygen and/or sulfur defects, yielding a lower-valence state. In addition, (iii) electron doping by F substitution leads to an increase in the lower-E_B peak, and (iv) the lower-E_B peak decreases with hole doping owing to Pb substitution in the F-substituted system. The Bi valences estimated by the line-shape analysis are listed in Table I. Furthermore, Fig. 4(b) shows Pb $4f$ core-level HAXPES spectra obtained at 200 and 50 K. In contrast to the Bi $4f$ core level, the spectrum has a single peak with strong asymmetry, in which the temperature-induced change is hardly visible except for the slight shift (∼30 meV). This shift would originate from the structural transition which induces the change in the potential at the Pb site. The Pb valences estimated by the line-shape analysis [shown in Fig. 4(d)] are also listed in Table I. They will be discussed later, along with the DFT results.

C. Valence-band HAXPES

To investigate the effects of element substitution and temperature variation on the electronic structures near E_F, we measured VB-HAXPES spectra. Figure 5 shows the spectra obtained with the *p*-polarized HAX. Compared to the SXPES [34], which is sensitive to S $3p$ states, the HAXPES shows an increase in intensity around 3–6 eV. For example, in the case of $LaO_{0.5}F_{0.5}BiS_2$, DFT calculations show that O $2p$ states dominate in this energy range; S $3p$ and Bi $6p$ bonding states are also present, as shown in Fig. 6. The intensity derived from the bonding states is enhanced in the *p*-polarized HAXPES spectrum because the photoionization cross section of the Bi $6p$ states is relatively large under the present experimental conditions [39].

As shown in Fig. 5, semiconducting $LaOBiS_2$ has a very weak peak near E_F, indicating that a small amount of electrons are doped into Bi $6p$ dominant bands as mentioned above. By substituting O for F, the peak develops and shifts to the higher E_B side by 180 meV (see inset for illustration), indicating electron doping in these bands. In contrast, for the Pb substitution, the peak was observed to shift 50 meV toward E_F owing to hole doping. These results support the interpretation that the change in the spectral shape of the Bi $4f$ core level due to F (Pb) substitution is attributed to electron (hole) doping.

As for the temperature dependence of the spectrum at $x = 0.09$, a slight change in the spectral shape was observed,

TABLE I. Bi and Pb valences in the BiS_2-based compounds. The nominal Bi valence is determined by assuming La^{3+}, O^{2-}, F^-, S^{2-}, and Pb^{2+} ions. Experimental values are estimated from Bi and Pb $4f_{7/2}$ core-level HAXPES spectra. Errors are attributed to the uncertainty of possible background. DFT values are derived from *s*-, *p*-, and *d*-orbital pDOSs integrated up to E_F in the atomic sphere.

		Bi valence			Pb valence		
Compound	T(K)	Nominal	HAXPES	DFT	Nominal	HAXPES	DFT
$LaOBiS_2$	50	3	2.82(4)	2.70			
$LaO_{0.5}F_{0.5}Bi_{1-x}Pb_xS_2$							
$x = 0$	50	2.5	2.54(4)	2.65			
$x = 0.09$	200	2.55	2.61(2)	-	2	2.48(2)	-
	50	2.55	2.63(3)	-	2	2.48(2)	-
$x = 0.125$	High-T phase	2.57	-	2.68	2	-	2.39
	Low-T phase	2.57	-	2.63	2	-	2.33

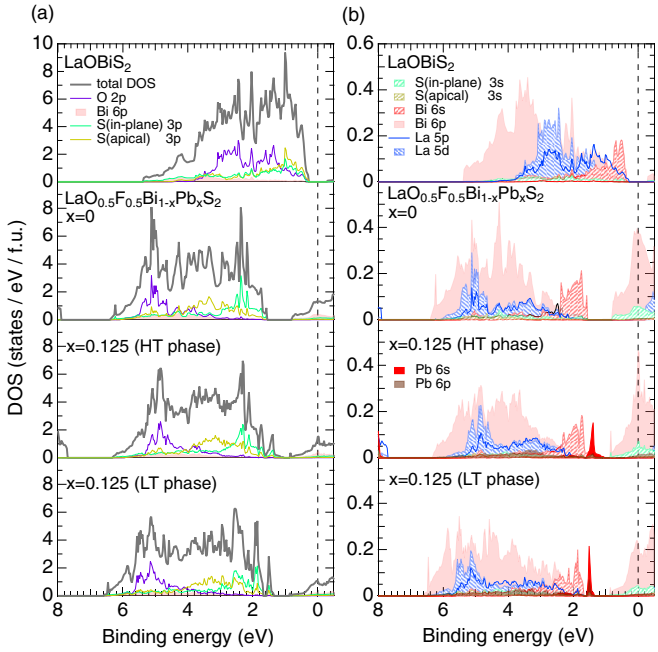

FIG. 6. Total DOS and some pDOSs of $LaOBiS_2$ and $LaO_{0.5}F_{0.5}Bi_{1-x}Pb_xS_2$. (a) Overall and (b) enlarged views.

accompanied by a shift of about 110 meV to the high E_B side in the low-T phase compared to the high-T phase, rather than a large change in the broad energy range as in the HERFD-XANES spectrum. This spectral shift is larger than those in the Bi $4f$ and Pb $4f$ core levels (60 meV and 30 meV, respectively) and is thought to reflect a change in the VB electronic structure with symmetry lowering caused by the structural phase transition to the low-T phase.

D. Mixed-valence state

Next, we discuss the validity of the experimentally obtained valences, which are summarized in Table I. To evaluate the Bi and Pb valences, we performed further DFT calculations for all other compounds and phases, whose DOSs are also shown in Fig. 6 [40]. Note that in the calculations, the percentage of Pb substitution was assumed to be 12.5% instead of the actual 9% to save computational effort for Pb-substituted systems. The valences estimated from the DFT results are also listed in Table I. Theoretical valences are obtained by the sum of integrated s-, p-, and d-orbital partial densities of states (pDOSs) up to E_F within the atomic sphere of 1.32 Å for both Bi and Pb atoms, which is greater than or equal to the ionic radii of octahedrally coordinated Bi^{3+}, Bi^{2+}, and Pb^{2+} ions [41,42]. The experimental value of the Bi valence in $LaOBiS_2$, which is closest to +3 in the three compounds, decreases to about +2.5 with 50% F substitution. This is in good agreement with the DFT prediction. While the Bi^{3+} state is the most chemically stable, the Bi^{2+} state has been reported to be stabilized in Bi-doped materials such as $Sr_2P_2O_7$:Bi^{2+} [43]. In contrast, to the best of our knowledge, mixed valence states of divalent and trivalent Bi have been found in very few materials such as Bi-doped zeolites [44]. Our results show that the mixed-valence states are realized in BiS_2-based compounds, which can lead to some charge-ordered structures and/or microscopic charge disproportionation [45]. Furthermore, the HAXPES captures the subtle increase in Bi valence caused by Pb substitution in the AP (i.e., high-T) phase, which is also reproduced by the DFT calculation. In contrast, the valence at 200 K is more or less the same as at 50 K, although it predicts a slight decrease with the phase transition. Although the electronic structure of Pb changes below 100 K, as seen in the Pb $L\alpha_1$ HERFD-XANES spectra, the valence of Pb does not change, unlike that of Bi. Under the assumption that the large (small) component in the spectrum shown in Fig. 4(d) is derived from the Pb^{2+} (Pb^{4+}) state, the mean valence is +2.48 [46]. On the other hand, it becomes +2.24 if the chemically unstable Pb^{3+} state possibly causes the small component.

Note that the above estimates are based on the assumption that all collected photoelectrons came from the bulk. At the surface, the Bi valence has been reported to be closer to +3 than in the bulk [47]. However, even assuming pure Bi^{3+} state at the surface, the influence of the surface on the estimates is within the errors owing to the high bulk sensitivity of HAXPES.

IV. SUMMARY

Taking advantage of the high energy resolution, we found that the HERFD-XANES spectra show a clear temperature change only in $LaO_{0.5}F_{0.5}Bi_{1-x}Pb_xS_2$ ($x = 0.09$), where bulk superconductivity is observed. This change is due to the symmetry lowering of the crystal at low temperatures, suggesting that the bulk superconductivity in the Pb-substituted BiS_2 compound is driven by a mechanism similar to that in the HP phase of $LaO_{0.5}F_{0.5}BiS_2$. The HERFD-XANES, core-level HAXPES, and VB-HAXPES spectra are consistently understood by the DFT calculations. With the help of the DFT calculations, Bi $4f$ core-level HAXPES revealed that the doped BiS_2-based compounds host a mixed state of divalent and trivalent Bi ions at the site of broken local inversion symmetry.

ACKNOWLEDGMENTS

We would like to thank Y. Murakami, Y. Arinaga, Y. Kondo, K. Oda, and M. Shimamoto for supporting the HAXPES experiments, A. Hariki for fruitful discussion, and M. Matsuki-Baltzer for providing support information. The HERFD-XANES and the synchrotron-XRD experiments at SPring-8 were performed with the approval of the Japan Synchrotron Radiation Research Institute (Proposals No. 2020A0630 and No. 2019A1347, respectively); the HAXPES experiments at SPring-8 were performed with the approval of RIKEN (Proposals No. 20190031, No. 20200075, and No. 20210068), under the support of JSPS KAKENHI Grants No. JP19K03753 and No. JP22K03527.

[1] R. P. Huebener, *History and Theory of Superconductors* (Springer Wiesbaden, Wiesbaden, 2021).

[2] M. Z. Hasan and C. L. Kane, Rev. Mod. Phys. **82**, 3045 (2010).

[3] Y. S. Hor, A. J. Williams, J. G. Checkelsky, P. Roushan, J. Seo, Q. Xu, H. W. Zandbergen, A. Yazdani, N. P. Ong, and R. J. Cava, Phys. Rev. Lett. **104**, 057001 (2010).

[4] X.-L. Qi and S.-C. Zhang, Rev. Mod. Phys. **83**, 1057 (2011).

[5] Y. Mizuguchi, S. Demura, K. Deguchi, Y. Takano, H. Fujihisa, Y. Gotoh, H. Izawa, and O. Miura, J. Phys. Soc. Jpn. **81**, 114725 (2012).

[6] G. R. Stewart, Rev. Mod. Phys. **83**, 1589 (2011).

[7] H. Usui, K. Suzuki, and K. Kuroki, Phys. Rev. B **86**, 220501(R) (2012).

[8] S.-L. Wu, K. Sumida, K. Miyamoto, K. Taguchi, T. Yoshikawa, A. Kimura, Y. Ueda, M. Arita, M. Nagao, S. Watauchi, I. Tanaka, and T. Okuda, Nat. Commun. **8**, 1919 (2017).

[9] X. Zhang, Q. Liu, J.-W. Luo, A. J. Freeman, and A. Zunger, Nat. Phys. **10**, 387 (2014).

[10] Y. C. Chan, K. Y. Yip, Y. W. Cheung, Y. T. Chan, Q. Niu, J. Kajitani, R. Higashinaka, T. D. Matsuda, Y. Yanase, Y. Aoki, K. T. Lai, and S. K. Goh, Phys. Rev. B **97**, 104509 (2018).

[11] K. Hoshi, R. Kurihara, Y. Goto, M. Tokunaga, and Y. Mizuguchi, Sci. Rep. **12**, 288 (2022).

[12] Y. Ota, K. Okazaki, H. Q. Yamamoto, T. Yamamoto, S. Watanabe, C. Chen, M. Nagao, S. Watauchi, I. Tanaka, Y. Takano, and S. Shin, Phys. Rev. Lett. **118**, 167002 (2017).

[13] K. Hoshi, Y. Goto, and Y. Mizuguchi, Phys. Rev. B **97**, 094509 (2018).

[14] Y. Mizuguchi, J. Phys. Soc. Jpn. **88**, 041001 (2019).

[15] K. Suzuki, H. Usui, K. Kuroki, T. Nomoto, K. Hattori, and H. Ikeda, J. Phys. Soc. Jpn. **88**, 041008 (2019).

[16] S. Demura, Y. Mizuguchi, K. Deguchi, H. Okazaki, H. Hara, T. Watanabe, S. J. Denholme, M. Fujioka, T. Ozaki, H. Fujihisa, Y. Gotoh, O. Miura, T. Yamaguchi, H. Takeya, and Y. Takano, J. Phys. Soc. Jpn. **82**, 033708 (2013).

[17] R. Jha, A. Kumar, S. K. Singh, and V. P. S. Awana, J. Appl. Phys. **113**, 056102 (2013).

[18] M. Tanaka, T. Yamaki, Y. Matsushita, M. Fujioka, S. J. Denholme, T. Yamaguchi, H. Takeya, and Y. Takano, Appl. Phys. Lett. **106**, 112601 (2015).

[19] K. Nagasaka, A. Nishida, R. Jha, J. Kajitani, O. Miura, R. Higashinaka, T. D. Matsuda, Y. Aoki, A. Miura, C. Moriyoshi, Y. Kuroiwa, H. Usui, K. Kuroki, and Y. Mizuguchi, J. Phys. Soc. Jpn. **86**, 074701 (2017).

[20] T. Tomita, M. Ebata, H. Soeda, H. Takahashi, H. Fujihisa, Y. Gotoh, Y. Mizuguchi, H. Izawa, O. Miura, S. Demura, K. Deguchi, and Y. Takano, J. Phys. Soc. Jpn. **83**, 063704 (2014).

[21] A. Yamashita, H. Usui, K. Hoshi, Y. Goto, K. Kuroki, and Y. Mizuguchi, Sci. Rep. **11**, 230 (2020).

[22] S. Otsuki, S. Demura, Y. Sakai, Y. Fujisawa, and H. Sakata, Solid State Commun. **270**, 17 (2018).

[23] S. Demura, T. Fukui, S. Kobayashi, C. Moriyoshi, K. Takase, Y. Kuroiwa, H. Sakata, and Y. Takano (unpublished).

[24] N. Kawamura, N. Kanai, H. Hayashi, Y. H. Matsuda, M. Mizumaki, K. Kuga, S. Nakatsuji, and S. Watanabe, J. Phys. Soc. Jpn. **86**, 014711 (2017).

[25] K. Hämäläinen, D. P. Siddons, J. B. Hastings, and L. E. Berman, Phys. Rev. Lett. **67**, 2850 (1991).

[26] M. Yabashi, K. Tamasaku, and T. Ishikawa, Phys. Rev. Lett. **87**, 140801 (2001).

[27] H. Fujiwara, S. Naimen, A. Higashiya, Y. Kanai, H. Yomosa, K. Yamagami, T. Kiss, T. Kadono, S. Imada, A. Yamasaki, K. Takase, S. Otsuka, T. Shimizu, S. Shingubara, S. Suga, M. Yabashi, K. Tamasaku, T. Ishikawa, and A. Sekiyama, J. Synchrotron Radiat. **23**, 735 (2016).

[28] M. Matsuki-Baltzer (private communication).

[29] P. Blaha, K. Schwarz, G. Madsen, D. Kvasnicka, and J. Luitz, *WIEN2k, An Augmented Plane Wave+Local Orbitals Program for Calculating Crystal Properties* (Technische Universitat Wien, Wien, 2001).

[30] R. Sagayama, H. Sagayama, R. Kumai, Y. Murakami, T. Asano, J. Kajitani, R. Higashinaka, T. D. Matsuda, and Y. Aoki, J. Phys. Soc. Jpn. **84**, 123703 (2015).

[31] P. Blaha, K. Schwarz, F. Tran, R. Laskowski, G. K. H. Madsen, and L. D. Marks, J. Chem. Phys. **152**, 074101 (2020).

[32] For the AP (HP) phase, we used the $\boldsymbol{k}$-point mesh of $11 \times 11 \times 3$ with 72 (115) irreducible $\boldsymbol{k}$ points for the $2 \times 2 \times 2$ supercell; the cutoff parameter, $R_{\mathrm{MT}}K_{\mathrm{max}}$, was set to 6.5 (7.0) for the minimum muffin-tin radius of 2.18 (2.01) bohr.

[33] D. A. Shirley, Phys. Rev. B **5**, 4709 (1972).

[34] S. Nagira, J. Sonoyama, T. Wakita, M. Sunagawa, Y. Izumi, T. Muro, H. Kumigashira, M. Oshima, K. Deguchi, H. Okazaki, Y. Takano, O. Miura, Y. Mizuguchi, K. Suzuki, H. Usui, K. Kuroki, K. Okada, Y. Muraoka, and T. Yokoya, J. Phys. Soc. Jpn. **83**, 033703 (2014).

[35] S. Tanuma, C. J. Powell, and D. R. Penn, Surf. Interface Anal. **43**, 689 (2011).

[36] M. Taguchi, A. Chainani, K. Horiba, Y. Takata, M. Yabashi, K. Tamasaku, Y. Nishino, D. Miwa, T. Ishikawa, T. Takeuchi, K. Yamamoto, M. Matsunami, S. Shin, T. Yokoya, E. Ikenaga, K. Kobayashi, T. Mochiku, K. Hirata, J. Hori, K. Ishii *et al.*, Phys. Rev. Lett. **95**, 177002 (2005).

[37] S. Chaturvedi, I. Sarkar, M. M. Shirolkar, U.-S. Jeng, Y.-Q. Yeh, R. Rajendra, N. Ballav, and S. Kulkarni, Appl. Phys. Lett. **105**, 102910 (2014).

[38] T. Nishikubo, Y. Sakai, K. Oka, T. Watanuki, A. Machida, M. Mizumaki, K. Maebayashi, T. Imai, T. Ogata, K. Yokoyama, Y. Okimoto, S. Koshihara, H. Hojo, T. Mizokawa, and M. Azuma, J. Am. Chem. Soc. **141**, 19397 (2019).

[39] M. B. Trzhaskovskaya, V. K. Nikulin, V. I. Nefedov, and V. G. Yarzhemsky, At. Data Nucl. Data Tables **92**, 245 (2006); $\theta = -30^{\circ}$ and $\phi = 180^{\circ}$ for our case.

[40] For $LaOBiS_2$ and $x = 0$, we used the $\boldsymbol{k}$-point mesh of $11 \times 11 \times 3$ for the unit cell; for $x = 0.125$ in both low-T and high-T phases, we used $9 \times 9 \times 5$ for the $2 \times 2 \times 1$ supercell. $R_{\mathrm{MT}}K_{\mathrm{max}}$ was set to 6.0–7.0 for these compounds.

[41] R. D. Shannon, Acta Cryst A **32**, 751 (1976).

[42] Some properties of the Bi^{2+} ion, including the ionic radius, have not been widely reported because of chemical instability. It is reasonable to assume that the radius of the Bi^{2+} ion is smaller than that of the Pb^{2+} ion, considering that the atomic radius of Bi is smaller than that of Pb.

[43] L. Li, M. Peng, B. Viana, J. Wang, B. Lei, Y. Liu, Q. Zhang, and J. Qiu, Inorg. Chem. **54**, 6028 (2015).

[44] Z. Bai, M. Fujii, T. Hasegawa, S. Kitano, K. Imakita, M. Mizuhata, and S. Hayashi, Opt. Mater. (Amsterdam) **34**, 821 (2012).

[45] T. Machida, Y. Fujisawa, M. Nagao, S. Demura, K. Deguchi, Y. Mizuguchi, Y. Takano, and H. Sakata, J. Phys. Soc. Jpn. **83**, 113701 (2014).

[46] Y. Sakai, J. Yang, R. Yu, H. Hojo, I. Yamada, P. Miao, S. Lee, S. Torii, T. Kamiyama, M. Ležaić, G. Bihlmayer, M. Mizumaki, J. Komiyama, T. Mizokawa, H. Yamamoto, T. Nishikubo, Y. Hattori, K. Oka, Y. Yin, J. Dai *et al.*, J. Am. Chem. Soc. **139**, 4574 (2017).

[47] K. Terashima, J. Sonoyama, M. Sunagawa, H. Fujiwara, T. Nagayama, T. Muro, M. Nagao, S. Watauchi, I. Tanaka, H. Okazaki, Y. Takano, Y. Mizuguchi, H. Usui, K. Suzuki, K. Kuroki, T. Wakita, Y. Muraoka, and T. Yokoya, J. Phys.: Conf. Ser. **683**, 012003 (2016).